

## Magnetic phase transition induced by electrostatic gating in two-dimensional square metal-organic frameworks

Yun-Peng Wang,<sup>1,2</sup> Xiang-Guo Li,<sup>1,2</sup> Shuang-Long Liu,<sup>1,2</sup> James N. Fry,<sup>1</sup> and Hai-Ping Cheng<sup>1,2,\*</sup>

<sup>1</sup>*Department of Physics, University of Florida, Gainesville, Florida 32611, USA*

<sup>2</sup>*Quantum Theory Project, University of Florida, Gainesville, Florida 32611, USA*



(Received 18 September 2017; revised manuscript received 11 January 2018; published 15 March 2018)

We investigate theoretically magnetism and magnetic phase transitions induced by electrostatic gating of two-dimensional square metal-organic framework compounds. We find that electrostatic gating can induce phase transitions between homogeneous ferromagnetic and various spin-textured antiferromagnetic states. Electronic structure and Wannier function analysis can reveal hybridizations between transition-metal  $d$  orbitals and conjugated  $\pi$  orbitals in the organic framework. Mn-containing compounds exhibit a strong  $d$ - $\pi$  hybridization that leads to partially occupied spin-minority bands, in contrast to compounds containing transition-metal ions other than Mn, for which electronic structure around the Fermi energy is only slightly spin split due to weak  $d$ - $\pi$  hybridization and the magnetic interaction is of the Ruderman-Kittel-Kasuya-Yosida type. We use a ferromagnetic Kondo lattice model to understand the phase transition in Mn-containing compounds in terms of carrier density and illuminate the complexity and the potential to control two-dimensional magnetization.

DOI: [10.1103/PhysRevB.97.115419](https://doi.org/10.1103/PhysRevB.97.115419)

### I. INTRODUCTION

Two-dimensional (2D) magnetism is a versatile area within condensed matter physics. Parent compounds of high- $T_c$  superconducting cuprates and iron pnictides exhibit 2D spin-textured antiferromagnetic states [1,2]. Anderson's spin liquid state [3] is realized in various 2D frustrated magnets, and transitions between magnetic phases underlies unconventional superconductivity [4] and the colossal magnetoresistance phenomenon [5]. Carrier density acts as a parameter for tuning magnetic phases where itinerant carriers are deeply involved in conducting magnetic interactions. Besides chemical doping, with doped manganites as examples [5], electrostatic gating, naturally suitable for 2D materials, is another approach for tuning carrier density hence the magnetic phase. Studies of phase diagrams and transitions of 2D magnetic materials deepen our understanding of 2D magnets and pave the way for their applications in spintronics.

The 2D metal-organic framework (MOF) has gained attention in the chemistry community with applications in gas separation and storage, optoelectric devices and membranes [6], and later in the physics community for magnetism in transition-metal-containing compounds [7]. 2D MOF magnets with square structure exhibit a more complex phase diagram [8] than those with triangular and kagome lattices; besides a geometrically frustrated state, square 2D MOF can also exhibit various antiferromagnetic states [8]. Square 2D MOFs consist of planar monomers covalently connected in both directions to form a 2D sheet. Monomers comprised of pyrrole-like units can form a coordination complex with transition-metal (TM) ions. Each TM ion hosts a local magnetic moment and magnetically interacts with its neighbors. For some 2D

MOFs their organic framework preserves  $\pi$  conjugation and carriers easily travel across boundaries and conduct magnetic interactions. The most studied of square 2D MOFs is TM embedded poly-pythalocyanine (TM-poly-Pc) [7,9–17], but the nature of magnetic interactions in these systems is not fully understood; the phase diagram remain largely incomplete [13], and magnetic patterns under electrostatic gating, a common and readily achieved experimental condition, are yet to be explored.

Hoping to stimulate experimental activity, we study the effect of electrostatic gating on magnetic phases of 2D square MOFs using a first-principles approach. Our results show that Mn-containing 2D square MOFs display electronic and magnetic properties very different from those containing other TM ions. Although the magnetic interactions in non-Mn-containing MOFs fit in the Ruderman-Kittel-Kasuya-Yosida (RKKY) picture, Mn-containing MOFs are described by the Kondo lattice model. In this paper we report results on three compounds, Fe-poly-Pc, Mn-poly-Pc and Mn-poly-TTP [TTP: 5,10,15,20-tetra(phenyl)porphyrin]. We discuss the origins of magnetic interactions by analyzing electronic and spin structure.

### II. COMPUTATIONAL METHOD

Calculations were carried out using the plane-wave pseudopotential approach of density functional theory (DFT) as implemented in the QUANTUM ESPRESSO package [18], adopting the Perdew-Burke-Ernzerhof parametrization [19] of the generalized gradient approximation. We employed pseudopotentials from the Standard Solid State Pseudopotentials (SSSP) library [20]. Plane-wave cutoff energies of 80 Ry and a  $5 \times 5 \times 1$   $k$  mesh were used to converge the total energies. A 15 Å-thick vacuum region was included in the unit cell to avoid the interactions between periodic images. The strong on-site

\*Corresponding author: [hping@ufl.edu](mailto:hping@ufl.edu)

correlations among  $d$  orbitals in TM elements were considered by including the Hubbard correction (DFT+ $U$ ) method [21] with  $U = 4$  eV and  $J = 1$  eV. The same values of  $U$  and  $J$  have been employed in previous studies on similar 2D MOF materials [9,10,17] and transition-metal phthalocyanine molecules [22]. Results for Mn-poly-Pc using a different set parameters ( $U = 5$  eV,  $J = 1$  eV) are presented in Appendix A. The effect of a gate voltage was applied by using the effective screening medium (ESM) approach [23], which imposes the electrostatic boundary conditions of a potential applied on the metallic gate on one side of the 2D system and vacuum on the other side.

### III. RESULTS AND DISCUSSIONS

Structures of TM-poly-Pc and TM-poly-TPP are schematically shown in Fig. 1. The lattice constant of TM-poly-Pc is 10.67 Å and for TM-poly-TPP is 17.80 Å. Each unit cell contains one TM ion at the center. Magnetic properties of these compounds can be represented by phenomenological Heisenberg model,

$$\hat{H} = J_1 \sum_{n.n.} \hat{S}_i \cdot \hat{S}_j + J_2 \sum_{n.n.n.} \hat{S}_i \cdot \hat{S}_k, \quad (1)$$

where  $\hat{S}_i$  is the spin operator of the TM ion on square lattice site  $i$ . Besides interactions among nearest neighbors ( $n.n.$ ), we also considered non-negligible interactions with next-nearest neighbors ( $n.n.n.$ ), which have been overlooked in previous studies [9]. We performed preliminary calculations using  $2 \times 2$ ,  $2 \times 3$ ,  $3 \times 3$ , and  $4 \times 4$  supercells, which indicate that magnetic interactions beyond the next-nearest neighbors are at least one order of magnitude weaker than  $J_1$  or  $J_2$ . These calculations also show that the values of  $J_1$  and  $J_2$  obtained from the total energies of FM, NAF, and CAF configurations

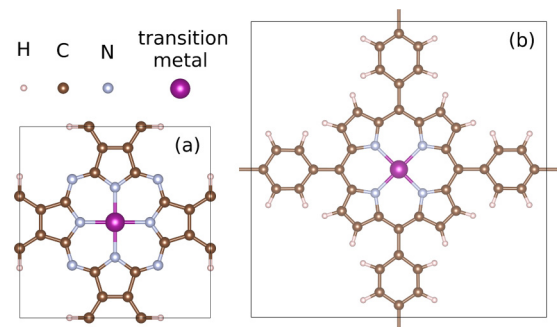


FIG. 1. Unit cell of transition-metal-embedded two-dimensional square (a) poly-pythalocyanine (poly-Pc) and (b) poly-(5,10,15,20-tetra(phenyl)porphyrin) (poly-TPP) metal-organic frameworks. The lattice constant is 10.67 Å for TM-poly-Pc and 17.80 Å for TM-poly-TPP.

[using equations (C4) and (C5)] agree well with those fitted from larger supercells.

The phase diagram of a system described by Eq. (1) is determined solely by the ratio between  $J_1$  and  $J_2$  [8]. In the classical limit, spin quantum number  $S \rightarrow \infty$ , the phase diagram consists of three states: a ferromagnetic state (FM) at  $|J_2| < |J_1|/2$  and  $J_1 < 0$ ; a Néel antiferromagnetic state (NAF) at  $|J_2| < |J_1|/2$  and  $J_1 > 0$ ; and a striped collinear antiferromagnetic state (CAF) at  $|J_2| > |J_1|/2$  [8]. Schematics of these magnetic states are shown in Fig. 2(g). In the quantum regime (small  $S$ ), spin-liquid states emerge at FM/CAF and NAF/CAF phase boundaries [8].

We calculate the total energies of the FM, NAF, and CAF magnetic configurations at different gate voltages, shown in Figs. 2(a)–2(c). At zero gate voltage, the lowest-energy

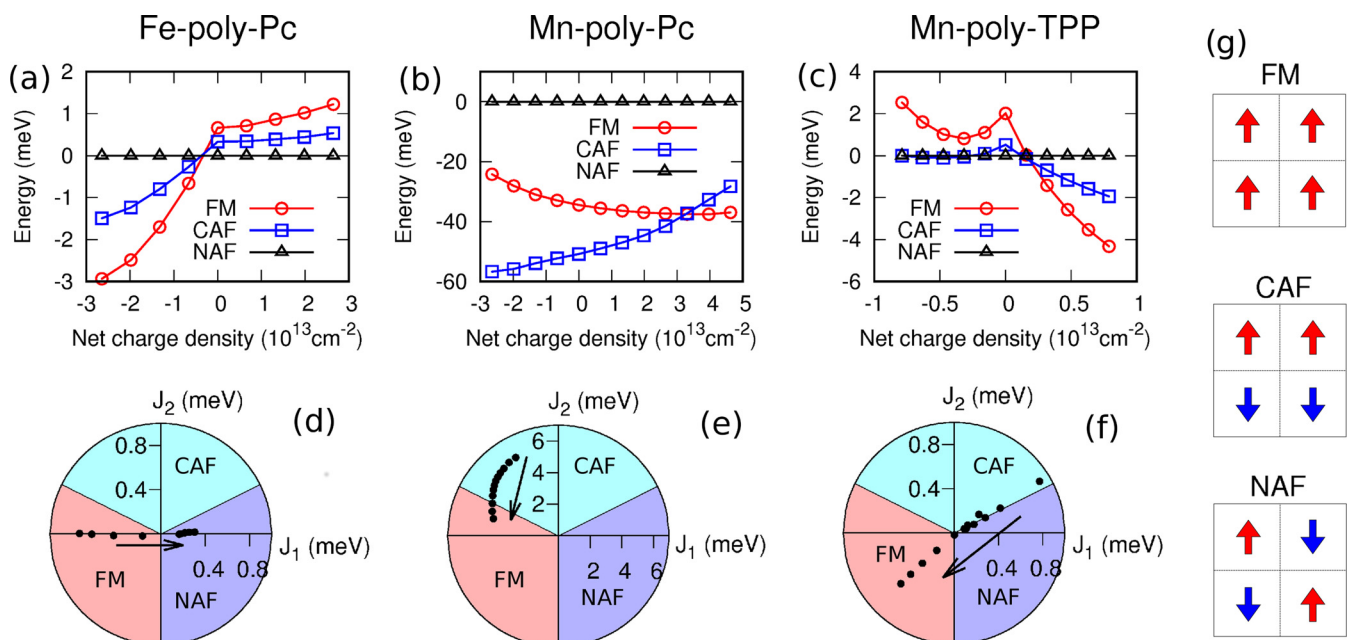


FIG. 2. DFT total energies of the ferromagnetic (FM, circles), collinear antiferromagnetic (CAF, squares), and Néel antiferromagnetic (NAF, triangles) configurations, for (a) Fe-poly-Pc, (b) Mn-poly-Pc, and (c) Mn-poly-TPP. Magnetic phase diagrams in the  $J_1$ - $J_2$  plane are shown in (d), (e), and (f). Arrows denote the increase of net charge density from negative (electron-doped) to positive (hole-doped). Schematic magnetic configurations are shown in (g).

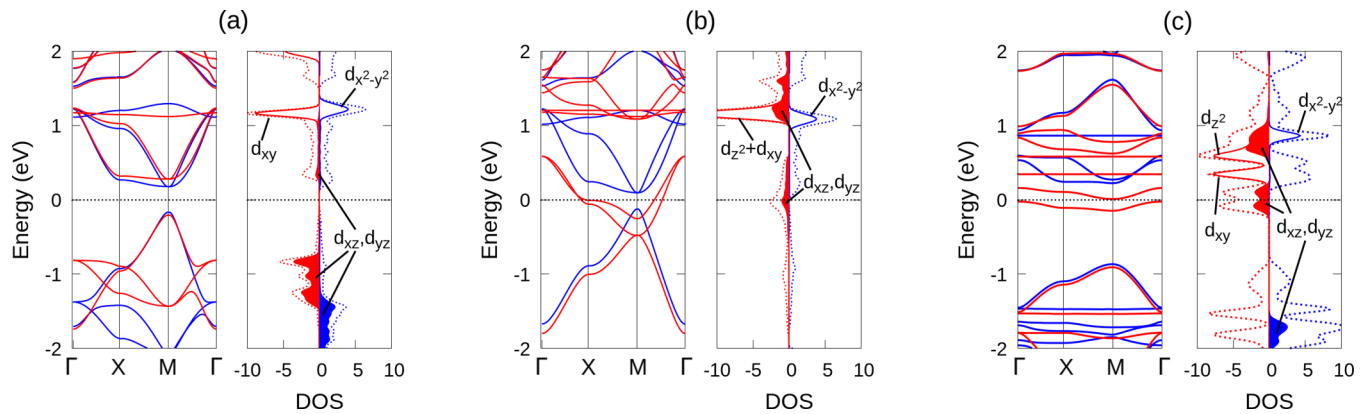


FIG. 3. The band structure (left panel) and density of states (right panel) of (a) Fe-poly-Pc, (b) Mn-poly-Pc, and (c) Mn-poly-TPP in the ferromagnetic configuration. Spin-up and spin-down channels are denoted as different colors. The total density of states is denoted by dashed lines, and that projected onto transition metal  $d$  orbitals by solid lines. The projected density of states on  $d_{zx}$  and  $d_{yz}$  are the same and are emphasized by the filled regions.

magnetic configuration is CAF for Mn-poly-Pc and NAF for both Fe-poly-Pc and Mn-poly-TPP. The relative energies of the FM, CAF, and NAF configurations change as a function of carrier density. For Mn-poly-Pc, the NAF configuration remains the highest, and FM becomes the ground state at hole density larger than  $3.5 \times 10^{13} \text{ cm}^{-2}$ . For Fe-poly-Pc, hole doping does not change the ground state, and the FM state becomes the ground state for electron doping. The CAF and NAF states have almost the same energy in Mn-poly-TPP under electron doping, while the FM state is the ground state for hole doping. Phase diagrams in the  $J_1$ - $J_2$  plane are illustrated in Figs. 2(d)–2(f). Values of  $J_1$  and  $J_2$  were calculated from total energies of FM, CAF, and NAF configurations. This figure summarizes the primary result of this work. We note that the FM state was regarded as the ground state for Mn-poly-Pc by previous studies in which the CAF spin configuration was not considered [9]. As one can see from Fig. 2(e), the magnetic coupling to next-nearest neighbors ( $J_2$ ) is of the same order of magnitude as the nearest-neighbor coupling ( $J_1$ ) and plays an important role.

Although the strength of magnetic couplings among TM ions is affected by the choice of  $U$  and  $J$  parameters, the magnetic phase transitions induced by electrostatic gating are not limited to the current set of parameters. Appendix A shows the results for Mn-poly-Pc using a different set of parameters where the same magnetic phase transition was observed.

Next we turn to the electronic and spin structure of 2D MOFs in order to understand the magnetic interactions in them. TM ions replace the two hydrogen atoms in Pc and TPP molecules, which makes TM in the 2+ valence state. The TM ions are in a square planar coordinate environment (see Fig. 1), which preserves the degeneracy between  $d_{zx}$  and  $d_{yz}$  orbitals. According to crystal field theory (CFT) [24], the  $d_{zx}$  and  $d_{yz}$  orbitals of  $\text{Mn}^{2+}(d^5)$  and  $\text{Fe}^{2+}(d^6)$  have the lowest energy among all the  $d$  orbitals, and the strong splitting of  $d$  orbitals in the planar square coordination leads to a low-spin ground state. For both  $\text{Mn}^{2+}$  and  $\text{Fe}^{2+}$  ions, four  $d$  electrons occupy the spin-down channel. The remaining one (two)  $d$  electrons of  $\text{Mn}^{2+}$  ( $\text{Fe}^{2+}$ ) occupy the  $d_{zx}$  and  $d_{yz}$  orbitals of the spin-up channel. As a result the spin-up  $d_{zx}$  and  $d_{yz}$  orbitals

of  $\text{Mn}^{2+}$  are half occupied. The CFT picture was verified by DFT+ $U$  calculations: magnetic moments of Mn and Fe ions in 2D MOFs are, respectively,  $3 \mu_B$  and  $2 \mu_B$ , and the energy splitting of  $d$  orbitals is as large as  $\sim 5 \text{ eV}$ .

Hybridization between the  $d_{zx}$  and  $d_{zy}$  orbitals of the TM ions and the itinerant  $\pi$  orbitals of the organic framework can be seen from the electronic structure. Because of hybridization, the density of states projected onto  $d_{zx}$  and  $d_{zy}$  orbitals is no longer in narrow peaks, but instead splits and smears substantially (Fig. 3). Fe-poly-Pc remains a semiconductor [Fig. 3(a)], as is the unsubstituted poly-Pc. Bands near the energy gap largely preserve their shapes in poly-Pc. The hybridization induces a slight spin splitting in both the valence and conducting bands of Fe-poly-Pc. In contrast, the hybridization leads to profound distortions in the band structure of Mn-poly-Pc, which becomes metallic, with two bands in the spin-up channel crossing the Fermi energy, as shown in Fig. 3(b). These two bands show strong energy dispersion with an energy band width of  $\sim 1 \text{ eV}$ , suggesting that they mainly originate from the conducting band of poly-Pc. Strong hybridization with the  $d_{zx}$  and  $d_{yz}$  orbitals is evidenced in the projected density of states, see Fig. 3(b). As a result,  $d_{zx}$  and  $d_{zy}$  orbitals of the  $\text{Mn}^{2+}$  ion in the spin-up channel become partially occupied, consistent with the CFT picture. The same thing happens for Mn-poly-TPP; see Fig. 3(c).

The electronic structure of Mn-poly-TPP is similar to Mn-poly-Pc if one looks closely. The two bands closest to the Fermi energy in the spin-up channel show almost the same dispersion, and the DOS at this energy range shows equal contributions from Mn- $d_{zx}$  and  $d_{yz}$  orbitals. So, a partial occupation of the spin-up band similar to Mn-poly-Pc is also present in Mn-poly-TPP. The similarity between Mn-poly-TPP and Mn-poly-Pc is also manifested in their phase diagram, where both become FM at hole-doping and AF at electron = doping.

The partial filling of  $d_{zx}$ - and  $d_{zy}$ -related bands is expected to induce a spontaneous breakdown of the degeneracy between them and hence a breakdown of the fourfold rotational symmetry of crystal structure. We performed structural optimizations using the FM configuration with a square-symmetry-broken starting geometry and also using the symmetry-breaking CAF

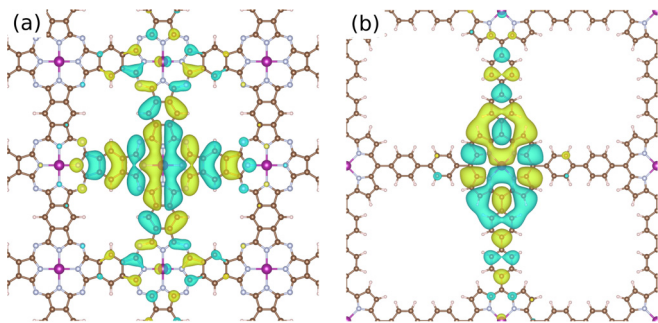


FIG. 4. Wannier function corresponding to the Mn- $d_{yz}$  orbital in (a) Mn-poly-Pc and (b) Mn-poly-TPP.

configuration. Calculation results show that the length of Mn-N bonds along the  $x$  direction are different by only 0.007 Å from those along the  $y$  direction, and the splitting of  $d_{zx}$ - and  $d_{yz}$ -related bands is negligible.

The hybridization between  $d$  orbitals of TM ions and  $\pi$  orbitals of organic framework is illustrated by Wannier functions (Fig. 4). The Hamiltonians of Mn-poly-Pc and Mn-poly-TPP were down-folded to the two bands closest to the Fermi energy in the spin-up channel. Results of the down-folding procedure include two Wannier functions corresponding to the two bands and hopping energies among these Wannier functions in different unit cells. The Wannier functions are centered at the Mn site, with one  $d_{zx}$ -like and the other  $d_{yz}$ -like. Only the  $d_{yz}$ -like Wannier function for Mn-poly-Pc and for Mn-poly-TPP are shown in Fig. 4; the  $d_{zx}$ -like Wannier function can be obtained by a 90° rotation of the  $d_{yz}$ -like. The Wannier function of Mn-poly-Pc spreads across the Pc monomer around the Mn ion and reaches as far as nearest-neighbor Mn ions, resulting in a hopping energy as large as 0.1 eV. The Wannier function of Mn-poly-TPP is not as delocalized as in Mn-poly-Pc, due to the larger lattice constant of Mn-poly-TPP, and the hopping energy between nearest-neighbor Wannier functions is about 30 meV. The difference between Wannier functions of Mn-poly-Pc and Mn-poly-TPP summarizes the difference in their electron structures and gives a clue to their different magnetic phases Fig. 2.

From electronic structure, we turn to the mechanism of magnetic interactions. The distance among TM ions is longer than 10 Å, so that atomic  $d$  orbitals from different TM ions do not overlap. Magnetic interactions can only be indirect. Various indirect coupling mechanisms were proposed and adopted in different materials. The Ruderman-Kittel-Kasuya-Yosida (RKKY) [25–27] mechanism was used to explain the magnetic interactions in dilute magnetic semiconductors [28] and in magnetic/nonmagnetic metallic multilayers [29]. The superexchange [30] and double-exchange [31] mechanisms were proposed to explain magnetic interactions in manganites and transition-metal oxides. Both the RKKY and double-exchange models involve a coupling between itinerant carrier spins and local magnetic moments, which forms one part of the Hamiltonian; the remaining part is the kinetic energy of itinerant electrons. The resulting Hamiltonian containing the Kondo term and the kinetic term is referred to as the Kondo

lattice model [32],

$$\hat{H}_{\text{Kondo}} = \sum_{ij,n} t_{ij,n} \hat{c}_{i\alpha,n}^\dagger \hat{c}_{j\alpha,n} + J_K \sum_i \mathbf{S}_i \cdot \sum_{\alpha\beta,n} \hat{c}_{i\alpha,n}^\dagger \boldsymbol{\sigma}_{\alpha\beta} \hat{c}_{i\beta,n}, \quad (2)$$

where  $n$  indexes itinerant electron bands;  $i$  and  $j$  are indices of lattice sites;  $\alpha$  and  $\beta$  are spin indices; and  $\mathbf{S}_i$  is the local magnetic moment on site  $i$ . Itinerant electrons are created by  $\hat{c}^\dagger$  and annihilated by  $\hat{c}$ . The single-band case was studied in Refs. [32–34], and the two-band case in Ref. [35]. The Kondo coupling  $J_K$  can be measured as the spin splitting of bands crossing the Fermi energy.

The oscillating RKKY magnetic interaction can be obtained by taking the weak coupling limit, which entails (i) a small Kondo coupling  $J_K$  compared to the band width of itinerant electrons, and (ii) a small number of itinerant carriers [35,36]. The opposite limit, taking the Kondo coupling to infinity and invoking the mean-field approximation, leads to the double exchange model [37]. The regime between the two limits needs sophisticated methods to account for the dynamical correlations [36].

As a semiconductor, Fe-poly-Pc has a small density of itinerant carriers even in the presence of electrostatic gating. As a result, Fe-poly-Pc fits in the RKKY picture. The same argument can be applied to all the 2D MOFs studied in this work except for Mn-poly-Pc and Mn-poly-TPP. The RKKY magnetic coupling coefficients are inversely proportional to the square of the distance between TM ions [38], which agrees with the much smaller value of  $J_2$  relative to  $J_1$  [Fig. 2(d)]. The RKKY coupling is proportional to the effective mass of the electron gas [39], which agrees with the opposite signs of  $J_1$  in electron- and hole-doping cases. Additionally, the RKKY coupling is proportional to the Kondo coupling  $J_K$ , which itself is proportional to the strength of the spin splitting of the conduction and valence bands. The magnetic coupling  $J_1$  among Cr ions in Cr-poly-Pc is stronger than that in Fe-poly-Pc, which agrees with the larger spin splittings of the conduction and valence bands. The larger spin splitting in Cr-poly-Pc is probably due to the larger magnetic moments of  $\text{Cr}^{2+}$  ions ( $4\mu_B$ ) compared with  $\text{Fe}^{2+}$  ions ( $2\mu_B$ ).

Mn-poly-Pc exhibit a much stronger hybridization that is manifested in the strong spin splitting  $\sim 0.5$  eV of the two bands crossing the Fermi energy [Fig. 3(b)]. Wannier functions corresponding to these bands, as shown in Fig. 4(a), exhibit substantial  $d_{zx}$  and  $d_{yz}$  contributions. The resulting strong spin splitting is due to the Hund's coupling with the other  $d$  orbitals forming the local magnetic moment. Indeed the spin splitting is on the same order of magnitude as the Hund's coupling of Mn ions ( $\sim 1$  eV) [40]. The phase diagram of the Kondo lattice model of Eq. (2) was studied using various methods [32–35]. The main result is that the FM phase is the ground state in the small electron density range, in accord with our results that FM becomes the ground state at large hole-doping region, see Figs. 2(b), 2(e).

A phase-separated state with coexisting electron-deficient FM and electron-rich AF domains was predicted for the Kondo lattice model [32]. However, we argue that the phase-separated state is not stable in Mn-poly-Pc. First, the Coulomb

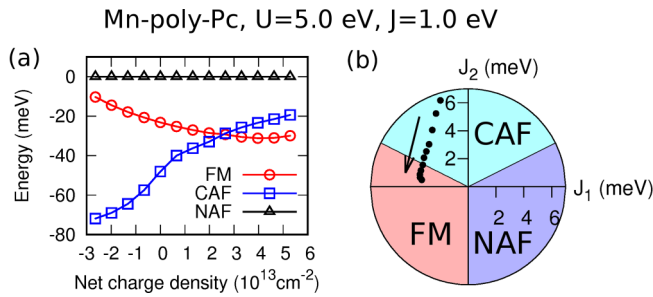


FIG. 5. Magnetic phase transitions in Mn-poly-Pc using the DFT+ $U$  method with  $U = 5$  eV and  $J = 1$  eV.

repulsion, especially the Coulomb tail, destabilizes macroscopic phase separation [41,42]; screening is largely weakened in 2D systems, which makes the situation more severe than in manganites and cuprates. Second, in doped manganites one can not exclude contributions from the inhomogeneity due to dopant ions. No such inhomogeneity exists in 2D MOFs studies in this work.

#### IV. CONCLUSION

We have investigated the magnetic phase transitions of 2D metal-organic frameworks under electrostatic gating using first-principles methods. Electrostatic gating is an efficient approach for tuning the magnetic order of 2D materials.

Analysis of electronic structure shows a strong hybridization between  $d_{zx}$ ,  $d_{yz}$  orbitals of transition-metal ions and the

$\pi$  orbital of the organic framework. The degeneracy of  $d_{zx}$ ,  $d_{yz}$  orbitals entails the partial filling of  $d_{zx}$ - and  $d_{yz}$ -related bands in Mn-containing compounds. The Kondo lattice model was adopted to understand the complex magnetic interactions in Mn-containing MOFs. The magnetic interaction in semi-conducting non-Mn-containing MOFs agrees with the RKKY mechanism. Our contributions are, (i) we have demonstrated that the magnetic phase transition induced by electrostatic gating can be engineered by changing the transition-metal ion or by changing the organic framework; (ii) we have revealed the microscopic mechanism of magnetic couplings and phase transitions in these materials; and we clearly show that magnetic coupling among next-nearest neighbors is not negligible in Mn-containing compounds.

#### ACKNOWLEDGMENTS

This work was supported by the US Department of Energy (DOE), Office of Basic Energy Sciences (BES), under Contract No. DE-FG02-02ER45995. Computations were done using the utilities of the National Energy Research Scientific Computing Center (NERSC).

#### APPENDIX A: MAGNETIC PHASE TRANSITIONS IN Mn-poly-Pc USING A DIFFERENT SET OF ( $U$ , $J$ ) VALUES

We performed DFT+ $U$  calculations on Mn-poly-Pc using  $U = 5$  eV and  $J = 1$  eV. The energies of different phases as a function of gate voltages [Fig. 5(a)] and the magnetic phase transitions induced by the gate voltage [Fig. 5(b)]

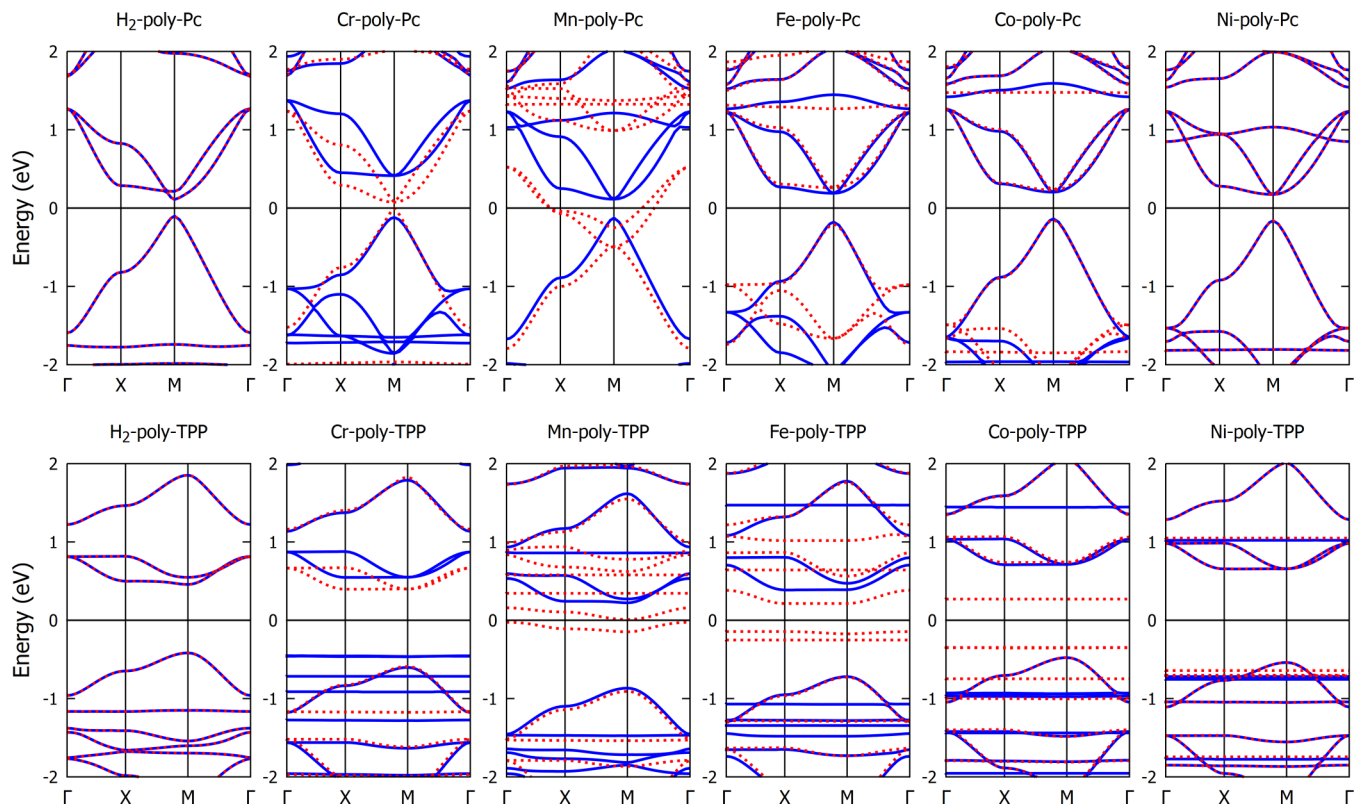


FIG. 6. Band structures of  $H_2$ -poly-Pc, TM-poly-Pc,  $H_2$ -poly-TPP, and TM-poly-TPP, with TM=Cr, Mn, Fe, Co, and Ni. TM-poly-Pc and TM-poly-TPP are in the ferromagnetic configuration.

are similar to Figs. 2(b), 2(e) in the main text, respectively. This additional calculation confirms that the magnetic phase transitions induced by gate voltages are not limited to the ( $U$ ,  $J$ ) parameters used in the main text.

### APPENDIX B: BAND STRUCTURES OF OTHER MOFs

The band structures of  $H_2$ -poly-Pc, TM-poly-Pc,  $H_2$ -poly-TPP, and TM-poly-TPP, with TM = Cr, Mn, Fe, Co, and Ni, are shown in Fig. 6. The calculated magnetic moments of TM ions are 4, 3, 2, 1, and  $0 \mu_B$  per  $Cr^{2+}$  ( $d^4$ ),  $Mn^{2+}$  ( $d^5$ ),  $Fe^{2+}$  ( $d^6$ ),  $Co^{2+}$  ( $d^7$ ), and  $Ni^{2+}$  ( $d^8$ ), in both TM-poly-TPP and TM-poly-Pc. By comparing the band structure of  $H_2$ -poly-Pc with TM-poly-Pc, we can understand the evolution of band structure with transition-metal ion substitutions. First, let us look at the energy band gap.  $H_2$ -poly-Pc is a semiconductor with a band gap of  $\sim 0.15$  eV. All TM-poly-Pc, except Mn-poly-Pc, are also semiconductors; the band structure of Mn-poly-Pc is discussed in the main text. Second, let us look at the dispersions of bands. Both the valence band and conducting band of  $H_2$ -poly-Pc are highly dispersive with a band width larger than 1 eV, which suggests that they originate from delocalized  $\pi$  orbitals of the organic framework. These highly dispersive bands are inherited by TM-poly-Pc, but their shapes are modified by strong hybridizations with TM- $d$  orbitals. Spin splitting induced by TM ions is commonly seen from the band structure. Bands of  $H_2$ -poly-TPP are less dispersive than those of  $H_2$ -poly-Pc. TM-poly-TPP shows spin splitting or addition of flat bands from TM ion  $d$  orbitals compared to  $H_2$ -poly-TPP.

### APPENDIX C: MAGNETIC PHASE DIAGRAMS

In this section, we present results for the Cr-containing compounds Cr-poly-Pc and Cr-poly-TPP.

We calculated the total energies of Cr-poly-Pc and Cr-poly-TPP in the ferromagnetic (FM), collinear antiferromagnetic (CAF), and Néel antiferromagnetic (NAF) configurations as a function of net charge density; see Figs. 7(a) and 7(b). Cr-poly-Pc [Fig. 7(a)] is similar to Fe-poly-Pc [Fig. 2(a) in main text], in that the FM state is the ground state on the electron-doping side and the NAF state is the ground state on the hole-doping side. Cr-poly-TPP [Fig. 7(b)] also exhibits the FM ground state on the electron-doping side; however, on the hole-doping side, all three states FM, CAF, and NAF of Cr-poly-TPP have the same energy, which can be explained by its band structure. Cr-poly-TPP is a semiconductor with a dispersive conduction band (originating from the organic framework) and a dispersionless valence band (originated from Cr ions), see Fig. 6. On electron doping, its Fermi energy moves upwards to the dispersive conduction band, and magnetic interactions can be effectively conducted by electrons of the organic framework. On the hole-doping side, its Fermi energy moves downwards, into the dispersionless valence band, which contributes little to magnetic interactions.

We can understand the Cr-poly-Pc and Cr-poly-TPP compounds using the model of Eq. (1) of the main text, writing the total energy as the sum of a term independent on magnetism, denoted as  $E_0$ , and two other terms corresponding to magnetic interactions among TM ions. The expression of the total

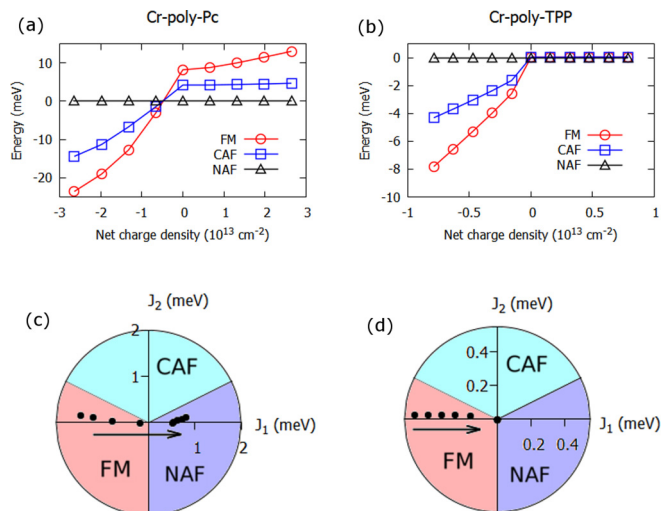


FIG. 7. Magnetic properties of Cr-poly-Pc and Cr-poly-TPP. Total energies of Cr-poly-Pc and Cr-poly-TPP in the FM, CAF, and NAF configurations are shown in (a) and (b), and magnetic phase diagrams in the  $J_1$ - $J_2$  plane of Cr-poly-Pc and Cr-poly-TPP are shown in (c) and (d).

energy at the FM, CAF, and NAF configurations [schematics of magnetic configurations are shown in Fig. 2(g) of the main text] are

$$E_{\text{FM}} = E_0 + 8J_1S^2 + 8J_2S^2, \quad (\text{C1})$$

$$E_{\text{CAF}} = E_0 - 8J_2S^2, \quad (\text{C2})$$

and

$$E_{\text{NAF}} = E_0 - 8J_1S^2 + 8J_2S^2. \quad (\text{C3})$$

where  $S$  is the spin quantum number at each TM site ( $S = 2$  for  $Cr^{2+}$  ions). The values of  $J_1$  and  $J_2$  can be calculated from  $E_{\text{FM}}$ ,  $E_{\text{CAF}}$ , and  $E_{\text{NAF}}$ ,

$$J_1 = \frac{1}{16S^2}(E_{\text{FM}} - E_{\text{NAF}}), \quad (\text{C4})$$

and

$$J_2 = \frac{1}{32S^2}(E_{\text{FM}} + E_{\text{NAF}} - 2E_{\text{CAF}}). \quad (\text{C5})$$

The values of  $J_1$  and  $J_2$  of Cr-poly-Pc and Cr-poly-TPP are plotted in Figs. 7(c) and 7(d). The similarity between Cr-poly-Pc [Fig. 7(c)] and Fe-poly-Pc [Fig. 2(d)] becomes clear. In fact, all three compounds, Cr-poly-Pc, Cr-poly-TPP, and Fe-poly-Pc share two features: first, as the electronic doping changes from electron doping to hole doping, the value of  $J_1$  evolves from negative to positive; and second, the value of  $J_2$  is always close to zero. Note that the Mn-containing compounds Mn-poly-Pc and Mn-poly-TPP, do not exhibit these two features.

- [1] P. A. Lee, N. Nagaosa, and X.-G. Wen, *Rev. Mod. Phys.* **78**, 17 (2006).
- [2] G. R. Stewart, *Rev. Mod. Phys.* **83**, 1589 (2011).
- [3] P. W. Anderson, *Mater. Res. Bull.* **8**, 153 (1973).
- [4] D. N. Basov and A. V. Chubukov, *Nat. Phys.* **7**, 272 (2011).
- [5] A. J. Millis, *Nature (London)* **392**, 147 (1998).
- [6] J. W. Colson and W. R. Dichtel, *Nat. Chem.* **5**, 453 (2013).
- [7] M. Abel, S. Clair, O. Ourdjini, M. Mossoyan, and L. Porte, *J. Am. Chem. Soc.* **133**, 1203 (2011).
- [8] N. Shannon, B. Schmidt, K. Penc, and P. Thalmeier, *Eur. Phys. J. B* **38**, 599 (2004).
- [9] J. Zhou and Q. Sun, *J. Am. Chem. Soc.* **133**, 15113 (2011).
- [10] J. Zhou, Q. Wang, Q. Sun, Y. Kawazoe, and P. Jena, *J. Phys. Chem. Lett.* **3**, 3109 (2012).
- [11] J. Zhou and Q. Sun, *J. Chem. Phys.* **138**, 204706 (2013).
- [12] Y. Li and Q. Sun, *Sci. Rep.* **4**, 4098 (2014).
- [13] J. Zhou and Q. Sun, *Nanoscale* **6**, 328 (2014).
- [14] Y. Wang, H. Yuan, Y. Li, and Z. Chen, *Nanoscale* **7**, 11633 (2015).
- [15] Q. Sun, Y. Dai, Y. Ma, X. Li, W. Wei, and B. Huang, *J. Mater. Chem. C* **3**, 6901 (2015).
- [16] M. Mabrouk and R. Hayn, *Phys. Rev. B* **92**, 184424 (2015).
- [17] W. Li, L. Sun, J. Qi, P. Jarillo-Herrero, M. Dincă, and J. Li, *Chem. Sci.* **8**, 2859 (2017).
- [18] P. Giannozzi *et al.*, *J. Phys.: Condens. Matter* **21**, 395502 (2009).
- [19] J. P. Perdew, K. Burke, and M. Ernzerhof, *Phys. Rev. Lett.* **77**, 3865 (1996).
- [20] K. Lejaeghere *et al.*, *Science* **351**, aad3000 (2016).
- [21] A. I. Liechtenstein, V. I. Anisimov, and J. Zaanen, *Phys. Rev. B* **52**, R5467 (1995).
- [22] I. E. Brumboiu, S. Haldar, J. Lüder, O. Eriksson, H. C. Herper, B. Brena, and B. Sanyal, *J. Chem. Theory Comput.* **12**, 1772 (2016).
- [23] M. Otani and O. Sugino, *Phys. Rev. B* **73**, 115407 (2006).
- [24] J. D. Lee, *Concise Inorganic Chemistry*, 5th ed. (Wiley-Blackwell, Hoboken, 1999).
- [25] M. A. Ruderman and C. Kittel, *Phys. Rev.* **96**, 99 (1954).
- [26] T. Kasuya, *Prog. Theor. Phys.* **16**, 45 (1956).
- [27] K. Yosida, *Phys. Rev.* **106**, 893 (1957).
- [28] T. Dietl, H. Ohno, F. Matsukura, J. Cibert, and D. Ferrand, *Science* **287**, 1019 (2000).
- [29] P. Bruno and C. Chappert, *Phys. Rev. Lett.* **67**, 1602 (1991).
- [30] P. W. Anderson, *Phys. Rev.* **79**, 350 (1950).
- [31] C. Zener, *Phys. Rev.* **82**, 403 (1951).
- [32] S. Yunoki, J. Hu, A. L. Malvezzi, A. Moreo, N. Furukawa, and E. Dagotto, *Phys. Rev. Lett.* **80**, 845 (1998).
- [33] A. Chattopadhyay, A. J. Millis, and S. Das Sarma, *Phys. Rev. B* **64**, 012416 (2001).
- [34] D. Pekker, S. Mukhopadhyay, N. Trivedi, and P. M. Goldbart, *Phys. Rev. B* **72**, 075118 (2005).
- [35] V. Michev and N. Karchev, *Phys. Rev. B* **76**, 174412 (2007).
- [36] A. Singh, A. Datta, S. K. Das, and V. A. Singh, *Phys. Rev. B* **68**, 235208 (2003).
- [37] G.-m. Zhao, *Phys. Rev. B* **62**, 11639 (2000).
- [38] M. T. Béal-Monod, *Phys. Rev. B* **36**, 8835 (1987).
- [39] V. I. Litvinov and V. K. Dugaev, *Phys. Rev. B* **58**, 3584 (1998).
- [40] A. Georges, L. de' Medici, and J. Mravlje, *Annu. Rev. Condens. Matter Phys.* **4**, 137 (2013).
- [41] E. Dagotto, *Nanoscale Phase Separation and Colossal Magnetoresistance: The Physics of Manganites and Related Compounds* (Springer, Berlin, 2013).
- [42] A. L. Malvezzi, S. Yunoki, and E. Dagotto, *Phys. Rev. B* **59**, 7033 (1999).